MP2 - A Novel Super-Resolution Image Analysis Tool to Assist in Unmasking the Structural Complexity of the Vaccinia Virion at Subviral Resolutions

Supervised by Jason Mercer & Ricardo Henriques

Word count: 4910

Ben K. Margetts

Abstract

The structure of the Vaccinia virion has been studied for over 70 years, however the acquisition of data on the location of its structural proteins, at subviral resolutions, has only recently become possible. Modern super-resolution microscopy tools are leading the way in allowing us to detail this structure, yet the computational tools required to analyse these datasets are limited. With this report, we present a novel image analysis tool to help unmask the structural complexity of the Vaccinia virion. We began by exploring scripts to extract viruses from image datasets, and progressed to normalizing, aligning, and comparing the structure of these viruses. Results suggest that structurally varied populations of virus are commonplace, and with this information we proceeded to produce an average structural model of the virus. This structural model will act as the starting point for future research endeavours; an aligned map for attaching the location of further fluorophore-labelled structural proteins to.

1 Introduction

Poxviruses from the large family *Poxviridae* are viruses known primarily for their infamous family member, variola. Variola is the causative agent of smallpox [1], thought to be responsible for some 300-500 million deaths in the 20th century before its eradication in 1979 [2]. Among the members of *Poxviridae* also lies Vaccinia, a live virus that is used as the key component of the naturally attenuated smallpox vaccine. Vaccinia is a well studied virus, frequented as a laboratory prototype for the study of its more infectious family members, and although we have been aware of Vaccinia for many years, the details of its uncommon viral structure still elude us. Genome sequencing of the virus, along with proteomic studies, have suggested that it consists of at least 75 viral proteins and 23 host proteins [3]. These proteins are encoded for by a surprisingly large 190-kb double-stranded DNA genome containing over 200 open reading frames, leading to initial expectations of a significantly larger proteome [4, 5].

The virus itself is a remarkably sizeable structure composed of a large centralised viral core containing viral proteins, enzymes, and the DNA genome. Two satellite-like lateral bodies lie adjacent to the viral core, and this set of structures are all contained within a viral envelope [6]. This structural complexity exhibited by Vaccinia and its family members is uncommon within DNA viruses, and is partially attributed to its unique extranuclear replication site within the cell cytoplasm [7]. Its large genome is thought to be needed for the production of a variety of proteins associated with gene transcription and DNA replication [8]. Briefly, during the virus's replication cycle, infectious forms of the virions can be produced: the intracellular mature virion, and the extracellular enveloped virion. Of these, the intracellular mature virion is the most abundant infectious form of the virus, and will be the focus of this paper.

To date, the vast majority of structural investigations into Vaccinia have taken place through a variety of electron microscopy (EM) methodologies, and more recently through the use of atomic force microscopy [9]. Vaccinia was first visualised in 1942 by EM [10] and since then, a large variety of EM techniques have been utilised in the study of the virus. These have included high voltage EM [11], deep-etch EM [12], and cryo-electron tomography [13] to name a selection. The virions are often described as being highly asymmetric and either brick-shaped, barrel-shaped, or ellipsoidal

in appearance [14], with approximate dimensions of 360 x 270 x 250 nm suggested by cryo-electron tomography measurements [13].

This viral structure is contained within two boundary-like elements, a lipid membrane that envelops the entirety of the virion with a thickness of approximately 5-6 nm [13], and two structural layers that contain the internal core of the virus. The outermost layer of this core wall consists of a random alignment of hexagonal spike patches, with the spikes appearing to be proteinaceous in nature, and anchored in the innermost lipid layer of the core wall [13]. This wall is estimated to be 18-19 nm thick and is significantly more complex in nature then would be expected [15]. At two distinct points in the virion, this core wall is separated from the membrane by the aforementioned lateral body structures [1]. These cylindrical proteinaceous structures are delivered alongside the core into the host cell during host-cell infection, and appear to act as 'delivery containers' for viral enzymes [16]. The structures themselves are disassembled within the host cell cytosol through proteasome activity, allowing the bound phosphatase, VH1, to dephosphorylate intracellular STAT1, preventing interferon-γ-mediated antiviral responses from taking place [16]. This process is likely to be very important for Poxviruses in establishing viral populations within a host, and highlights the importance of the lateral body structures for viral function.

Another aspect of Vaccinia's structure that demonstrates complexity, is its storage of the DNA genome. Contained within the viral core, the DNA genome displays evidence of secure storage, as it is intertwined within helical tubes 30-40 nm in diameter [17, 14]. When treated with proteases, these tubes are degraded, revealing 16 nm fibres that appear to coat the supercoiled DNA [6]. The functional relevance of this controversial finding appears to be linked to compacting the genome, suggesting that although the virus is large, it utilises its biomass efficiently.

The DNA genome encodes a large variety of structural and functional proteins for the virus. Of the potential 75 viral proteins, 65 have consistently been detected within intracellular mature virions with at least 22 proteins having been localised to the viral membrane [18]. Of these 22 proteins, it appears as though only 2 are enzymatic, with the remaining 20 acting as structural proteins, a significant number for a virus. 47 of these proteins have also been identified within the core fraction of the virus, however this fraction, produced by reducing the virus with an assay, contains both the viral core and lateral bodies [19]. Only 19 of these are not identified as having any enzymatic function, and very few of them have been further localised to a specific sub-structure within the core fraction. Those that have, required significant work to localise using standard cell biology tools [20].

In 2006 this accumulated structural data was amalgamated to produce a rudimentary 3D model of the Vaccinia virion [1]. The majority of these data, as mentioned previously, are produced through EM imaging and proteomic studies, with the key limiting factor in these investigations being the optical resolution available to us. It is a relatively simple task to bind a fluorescent molecule to a specific viral protein and image its location on the virus, however the issue here lies in the resolvable point spread function given by the excited fluorescent molecules. With traditional tools such as confocal microscopy, the diffraction limit of light simply doesn't allow us to resolve the sub-viral position of a specific viral protein, however with newer super resolution imaging techniques, this limit is being slowly overcome. This report will focus on the application of 2D structured illumination microscopy (SIM) to this issue. SIM utilises a structured light pattern to illuminate the sample and increase the spatial resolution by measuring the fringes in this projected Moirè pattern. Information from the frequency space outside of this observable region is collected through the Fourier transform of the spatial function projected. The phase of this Fourier transform is then separated and reconstructed, with the reverse of the Fourier transform returning a super-resolution image with a theoretical spatial resolution limit of 100 nm in the x, y plane and 200 nm resolution in the z plane [21].

With super resolution microscopy, we can begin to construct a new structural model of Vaccinia, and using computational tools, begin to localise structural proteins to specific viral substructures at sub-viral resolutions.

2 Materials & Methods

2.1 Materials & Data Collection

The program presented with this report was written for use with the Fiji distribution [22] of the ImageJ platform (version 2.0.0-rc-24). Scripts for the platform's 'macro' functionality were written primarily in Jython (version 2.7b) and Python (version 2.7.7), calling a variety of Java libraries (version 8, update 40), and inbuilt ImageJ functions. The software was first tested on a set of pre-existing SIM .tif images. Following this, 2D and 3D SIM images were collected from a Zeiss Elyra PS.1 system at room

temperature, specifically for the purpose of testing the program. When collected from the Elyra system, some image pre-processing was required to construct a SIM image from Zeiss's proprietary file format (.czi) using the Zeiss Zen software package (Service Pack 2). Throughout this report, lateral bodies are demonstrated with green fluorescent protein bound to the lateral body protein F17, and viral cores with with the EGFP-mCherry stain bound to the core protein A4 [16].

2.2 Program Design

The program was designed to begin by taking two images as input, an image of the flurophore-labelled viral cores, and an image of the flurophore-labelled lateral bodies. If these two images were acquired together in one file, then the user could easily split the image by channel, separating the labelled lateral bodies and viral cores into two files (see figure 1).

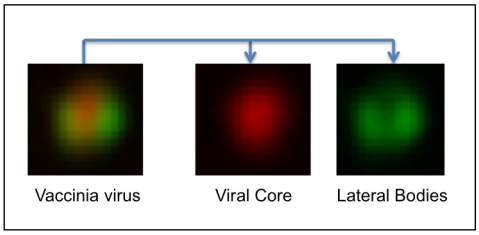

Figure 1: Fluorescence labelled Vaccinia structures split by channel.

The program then proceeds to detect expected viral features within the image. It does this by first blurring the image by a Gaussian function, in an attempt to smooth out the returned point spread function from the image acquisition system. This theoretically reduces the noise in the image, creating defined central peaks of fluorescence intensity on viral structures (see figure 2). The Gaussian function used in these images is defined as:

$$g(x) = \frac{1}{\sqrt{2}\pi\sigma} e^{-0.5}$$

where σ represents the user defined radius of decay.

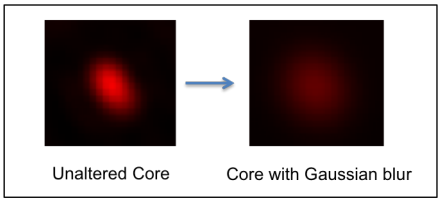

Figure 2: Gaussian blur function, where $\sigma = 3$, applied to a viral core.

After this has been applied, the program then runs an ImageJ function (Find Maxima) to extract the locations of pixels with peak intensity values. This is filtered by an image noise threshold that is defined by the user. This function returns a vector of x,y values, detailing the position of these peak intensities across the image's x,y plane, which can then be used to create a new image based on a rectangular selection taken around those coordinates. Each of those images thereby theoretically details a single viral structure, which can then be organised into a stack of images (see figure 3).

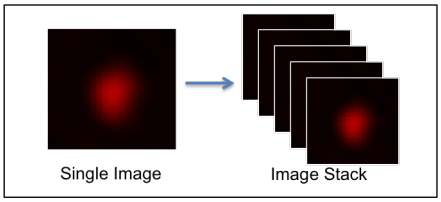

Figure 3: Visual representation of image stacks.

In an ideal image stack, each individual image, or slice, would contain a single viral structure, however this is not the case in many scenarios. Vaccinia virions can tend to clump together, and can naturally overlap in dense cultures, leading to slices containing multiple virions, biasing comparative analyses. This issue was approached in two separate ways, filtering out all possible slices where these scenarios present. For viral cores, the filter removes all slices where two image peaks are identified within the numerical image size values that are provided by the user, and for lateral bodies, it looks for two closely located image peaks to match. When these are located, it defines a central point between these two peaks, approximating the centre of the viral core within the lateral bodies; all unmatched lateral bodies are removed. This filtering methodology effectively removes beads, anomalies, and non-normally orientated viruses from the stacks. For example, if a virus happens to be imaged from a side-on orientation, only one lateral body will be visible, and may be centrally aligned with the viral core (see figure 4), obscuring the fluorophores from the objective lens.

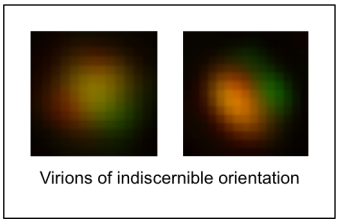

Figure 4: Virions for which an orientation cannot be determined.

Following this, an environment is initialised for normalizing the pixel intensity values of the filtered images. The images are normalized by returning a

numerical array of intensity values from each image, extracting the minimum and maximum values from this array, and running the following simple image normalization function over each position in the array:

$$f(Val) = \frac{Val - Min}{Max^{-2}}$$

where Val is the intensity value for the current pixel, Min is the minimum pixel intensity value for each array, and Max is the corresponding maximum pixel intensity, giving an array of integers between 0 and 100. These arrays are then returned to the image processor, producing images of normalized virions (see figure 5).

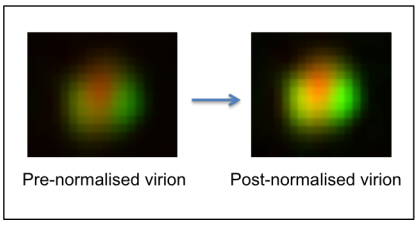

Figure 5: Virion pre and post normalization comparison.

At this point, the filtered stacks of viral structures are ready to be associated with each other. Here, the coordinates of filtered viral cores are matched with the central coordinates of filtered lateral bodies, allowing for a small shift in x and y to account for any chromatic aberrations presented by the microscope's objective lens. Any unmatched slices are discarded, and the resulting pairs are coerced from individual 16-bit image processors into combined RGB-colour processors, containing the matched viral core and lateral bodies centred by the intensity-defined centres of the structures.

Whilst in this stage of the program, the merged stacks contain sets of matched, filtered virions that cannot be analysed due to their random alignment. Each image must therefore be manipulated so that they lie in vertical alignment based upon the position of each virion's major axis. Two alignment methodologies were trialled in our program to tackle this issue, virion alignment by viral core standard deviations, and virion alignment by relative lateral body location.

The first alignment methodology: viral core alignment, begins by returning to the filtered viral core stack, and extracting each viral core slice in-turn. A thin rectangular selection, the height of the image and 1 pixel wide, is then positioned centrally on the image, so that it lies vertically across the midpoint of the slice. The standard deviation of this rectangular selection is then calculated and stored in an array, before the selection is rotated by a user defined value. This process is then repeated until the selection has rotated 180 degrees on its point of origin, where the major axis is given as the angle of rotation required to return the greatest standard deviation, and the minor axis is given as the angle of rotation required to return the lowest standard deviation (see figure 6). If this method of alignment is selected, the major axis angle is then used to rotate the image processor for the corresponding matched core and lateral bodies, theoretically aligning all matched virions along their major axis.

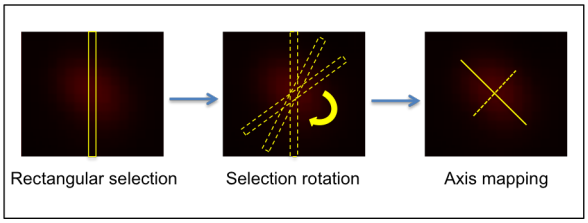

Figure 6: Visual representation of viral core alignment.

The second alignment methodology: lateral body alignment, utilises the central peak of each individual lateral body to align the two. Once the lateral bodies have been filtered, it can be assumed that the peak point of each lateral body is roughly equivalent to the centre of its structure. Therefore, if there are two guaranteed detectable intensity peaks in every image, we can use this information to align the virions. This process is initialised by returning the coordinates of both peaks, and then drawing a line between them. The angle of this line is then used to calculate the angle that the virion is aligned to (see figure 7). The image processor for the corresponding virion is then simply rotated by this amount, vertically aligning it.

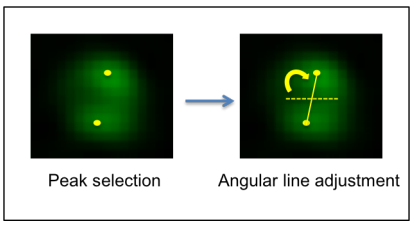

Figure 7: Visual representation of viral lateral body alignment.

After viral alignment, the images can be coerced into a base structural model of the virus. The program achieves this through a z-projection of the aligned image stack. This z-projection calculates the average intensity value for each pixel in the x, y plane from a vector of values taken from the z plane of the aligned image stack. These averaged values are then used to create a reconstructed image of the average virus from the information derived from raw SIM images (see figure 8).

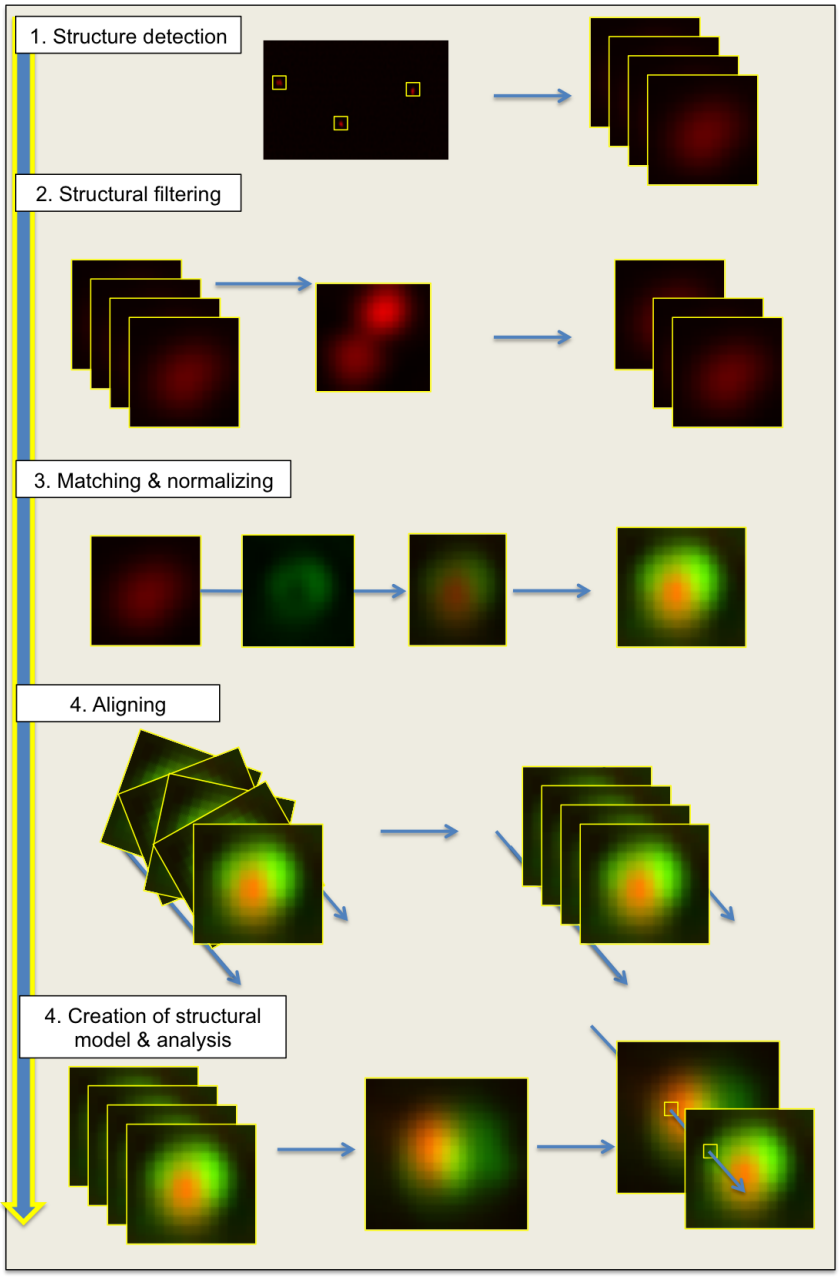

Figure 9: Flowchart demonstrating program design.

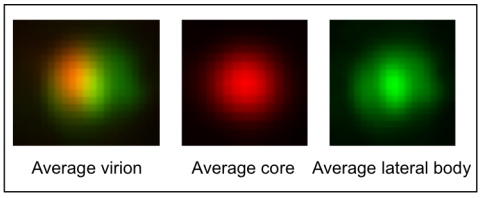

Figure 8: Example z-projections.

Following the creation of this structural model, each slice in the image stack can be compared against the average virus to obtain an estimation of the intra-viral variation. For this comparison, the mean-squared error metric was utilised due to the weighting it places on outlying values. The mean squared error (MSE) for this program is defined as:

$$\frac{1}{n}\sum_{i=1}^{n}(X_i - Y_i)^2$$

where n represents the number of slices in the stack, X_i gives the pixel intensity values obtained from the structural model, and Y_i gives the observed pixel intensity values obtained from the image slices.

This program is accessible to the end-user from a graphical user interface (GUI), where the user can modify a variety of the parameters discussed previously, and can enable/disable some of these image processing steps, i.e. the filtering, matching, nor-

malization, and z-projections, to match their desired output.

3 Results & Discussion

3.1 Detection & Filtering

Out of 25 test datasets (comprising of 1 viral core image and 1 lateral body image per set), the program was able to detect all visible viral structures in 23 of these datasets following the implementation of some minor parameter adjustments. Issues didn't tend to present through virions remaining undetected, but instead presented through how sensitive the detection methodology was to extracting anomalous data such as imaging beads, and minor fluctuations in pixel intensities.

The techniques that we utilised to filter anomalous selections from these datasets proved exceptionally effective, frequently removing over 50% of all selected points. The results obtained with these filtering and extraction tools are inherently variable, and based primarily upon the users parameter selection choices; however in our general experience, when calibrated effectively, the program didn't pass a single non-viral structure through the filter, and only occasionally passed images through where multiple virions were present (see figure 10). These cases tended to be isolated, and primarily caused by the threshold ranges given to the Find Maxima function, where the program simply hadn't registered a second virion structure as being present in the image, due to its intensity peaks falling below the user-defined thresholds. Issues did arise when the program was subjected to non-ideal datasets, where very large populations of the virus crowded the image, or where issues with fluorophore binding lead to inconclusive results.

Although the specificity of these filtering techniques bordered on exclusive, rather than inclusive, we feel that this is a minor flaw, given the high quality datasets that it can produce. Within the context of this area of research, many images can be taken per experiment within a relatively short timeframe, meaning that there is no shortage of datasets that can be fed into the program, and therefore no shortage of output. We feel that the use of such specific filtering strategies is instead flawed in the sense that it is not directly applicable to other families of virus, meaning that use of this program is, at least initially, limited to the study of Vaccinia.

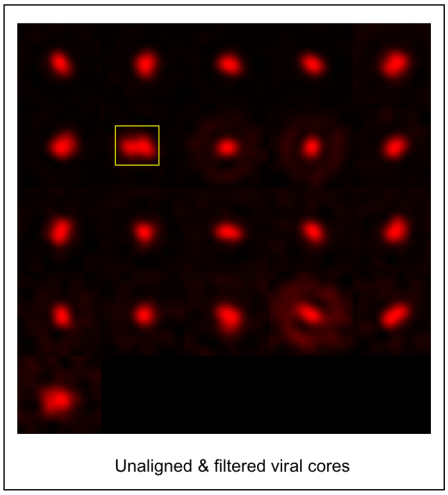

Figure 10: Representative filtered output from program with potential anomaly highlighted.

3.2 Centering & Alignment

Manual centering of matched viral and lateral bodies was frequently found to be necessary even in SIM images that were preprocessed to remove chromatic aberrations (with the Zeiss Zen software package). Subjectively based off of the appearance of image outputs, our rudimentary centering technique appears to be somewhat effective in reducing the appearance of chromatic aberrations (see figure 11), although is prone to errors, and relies purely on the structure of the virions for its effectiveness.

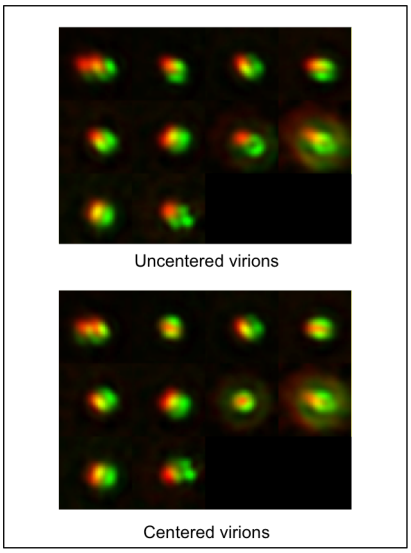

Figure 11: Uncentered virions compared to centered virions.

Issues with this technique revolve around its potential to centre a viral core and pair of lateral bodies together, that are not associated with each other. This would likely arise in cases where the viral matching ranges are set at higher levels than

default, and is relatively unlikely. Occurrences of this issue would also be relatively easy to identify from the misaligned rotations that would be applied to the viral core and the lateral bodies in the alignment stage.

The two alignment methodologies that we trialled with this program produced drastically different results. The first, viral core alignment, proved to be surprisingly ineffective at determining the rotations that needed to be applied to the virions. Its estimations of major and minor axis placement varied wildly between virions, with a mean angle of 67 degrees $\pm$ 39 between the two axis. From the results, it is clear that viral core alignment misrotates a large number of the virions, and takes a significant portion of the overall computation time for the program (approximately 56% of the overall computation time on a 2.7 Ghz Intel Core i5 iMac). We attribute these errors in viral core alignment primarily to the non-Gaussian intensity spreads commonly exhibited by EGFP-mCherry labelled viral cores. Ideally, when these cores are labelled, the fluorescence emitted would be detected in the form of a Gaussian point spread function from the centre of each flurophore, however this also assumes that the stains are evenly bound across the surface of the core. In images we have collected, this assumption is often incorrect, with uneven pixel intensities visible across the viral core, leading to uneven, and incorrect alignment measurements.

The alternative alignment methodology that we trialled, lateral body alignment, proved to be significantly more effective at consistently aligning sets of virions in comparison with viral core alignment (see figure 12). Computationally, lateral body alignment was also a substantial improvement over viral core alignment, reducing computation time by an approximate 41% on test data. Negatives associated this technique are centred around its reliance on lateral body structure and peak detection. This technique, although an improvement, is still far from the consistency required for such a technique, for example: if the centre of a lateral body is incorrectly located, then the virion will be misaligned by the program in every instance. This is further impacted by the constraints that this alignment technique places on the end-user, as for it to be enabled, the lateral bodies must be filtered to ensure that two lateral body centres can be located in each image. This constraint is not required with viral core alignment, and therefore produces two separate recommendations: the use of filtered lateral body alignment is recommended in all cases where there are enough datasets to facilitate the loss of data through lateral body filtering, and in cases where data is limited, we recommend unfiltered viral core alignment to generate the greatest possible amount of output.

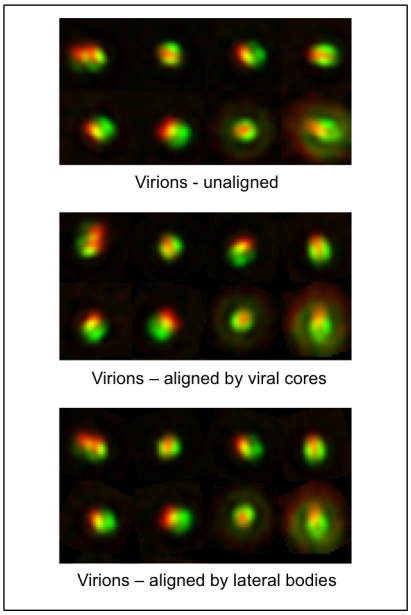

Figure 12: Comparison of virion alignment techniques.

3.3 Structural Models

From our relatively simplistic technique for generating structural models of the average Vaccinia virion within viral populations, some interesting results were revealed. We calculated the MSE of pixel intensity values between filtered virions, and the averaged structural model, for both viral cores and lateral bodies. The results of these measurements, taken from the most representative image sets, are summarised in figure 13.

Virion	Lateral Body MSE	Core MSE
1	86	17
2	74	19
3	50	18
4	116	31
5	70	92
6	103	26
7	90	10
8	231	16
9	175	12
10	141	33
Average:	113.6	27.4

Figure 13: Mean squared error of viral cores and lateral bodies.

These data, at first glance, suggest a striking differ-

ence in structural variation between the viral cores and lateral bodies, with lateral bodies exhibiting significantly more variation from the model then the viral cores. There is little-to-no evidence of structural variation within the literature-base to support these claims, however this lack of data can be explained by the methodologies used in previous studies, where access to these structures was limited by resolution and visibility. There is a difference in recorded size of whole virions within the literature [1], however this can be explained through variations in how the virus was prepared for imaging, and also through the techniques used to image the virus. There has simply been very little study on intra-virion variation within a viral population, which leaves us unsure on the validity of this result. This same result is repeated across numerous datasets, yet the confidence that can be placed in some of these results is limited by the quality of the SIM image. Based on this, we have started contemplating whether this structural variation could potentially be advantageous in nature, however there doesn't appear to be much supporting evidence for this hypothesis. Advantages in virion variation tend to lie in structural plasticity, where a host's innate immune response is evaded through the plasticity exhibited by the virus, or where faulty viral replication leads to significant changes in viral structure, again leading to successful evasion of the immune response. These advantages don't appear to logically correlate with the structural variation suggested by these data, as the lateral bodies are contained within the outer viral envelope, and therefore are only likely to interact with the immune system indirectly as discussed earlier.

Plausible explanations for this variation can instead be presented based on the fundamental principles this program is built on. To begin with, although our filtering system accounts for side-orientated viruses, it is possible that within these cultures, a small percentage of virions are orientated in such a way that both lateral bodies are visible, but the virus is still tilted to the side. In this scenario, a reduced body of fluorescence would be visible and would therefore result in a visual representation of one smaller lateral body, and one larger lateral body, which would differ significantly from the average lateral body projection. Another plausible explanation for this phenomena is based on the z-projection technique used for creating the structural model. This technique assumes that each structural element is aligned along an identical axis, whereas in reality if this axis is even slightly incorrect, the pixel to pixel comparison outside of the centre of the virion would be unrepresentative, increasing in misrepresentation the further out from the centre that you measure. In the case of the lateral bodies, this would lead to strong fluorescence from the centre of a lateral body being compared against the less intense edge of the model lateral body. This, combined with the issues presented through incorrectly centred structures, leads to a less defined gap between the two lateral bodies (see figure 14), thereby accounting for the varied mean squared errors presented where intensity differences exhibited between individual lateral bodies don't fit the profile of the averaged datasets.

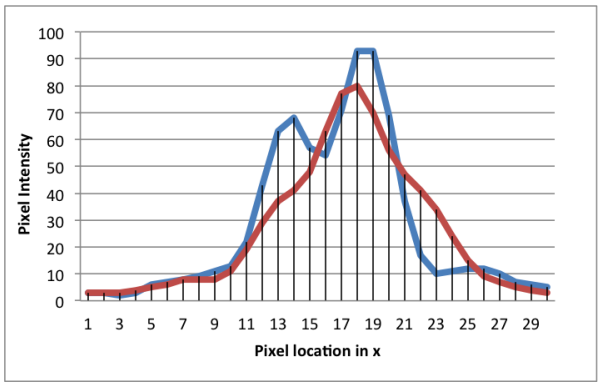

Figure 14: Horizontal pixel slice from a single pair of lateral bodies (blue) against model data (red).

This issue is potentially a symptom of the relatively small amounts of structures used for model creation, where outliers take up a significant portion of the dataset, skewing the important intensity distinction exhibited between lateral bodies. As this overall structure can be assumed to be constant within the Vaccinia virions, a potential progression from this point could be to filter numerical outlying pixel values from the datasets, and class those as misaligned/incorrectly centred structures. Another solution in data-rich landscapes, would be to extend this z-projection technique over very large image stacks containing many virions. In these large datasets, outlying values may be outweighed by values that fall within normal ranges, and the data that defines these average structures may begin to convene on two defined peaks, allowing for stronger comparisons with individual virions.

Based on these findings, an argument could be made that the MSE is an inappropriate metric to use, as the datasets contain outlying values that give large differences between the model and actual data. The MSE will therefore place an exponentially greater emphasis on these errors due to the method used to calculate the metric, and is likely to highlight these over structurally varied virions. Although this is true for these test datasets, if either of the previous suggestions are implemented, the mean squared error could be a valuable metric

for measuring this difference between the observed data and the model. Adjustments to these metrics could not be produced for this report due to time constraints.

3.4 Strengths & Limitations of the Program

We believe that the strengths of this program are demonstrated by what it achieves in comparison with the initial aims of the project. The software is a product of the overarching goal to engineer the codebase needed for localising proteins to Vaccinia sub-structures at sub-viral resolutions. A key strength of it lies in its usability and dynamic GUI (see figure 15), where the user can select from a variety of options to display very specific configurations of virus, allowing the program to be useful for automating basic feature extraction tasks that are time consuming for wet-laboratory scientists. The limitations with the program are currently most evident in the alignment and centering portions of the code, where erroneous data can be produced. The structural models it produces of viral cores tend to be reasonably accurate, yet lateral body models are less representative. Other limitations with the program include occasional software-bugs, and unnecessary long computation times due to the higher-level language it was written in.

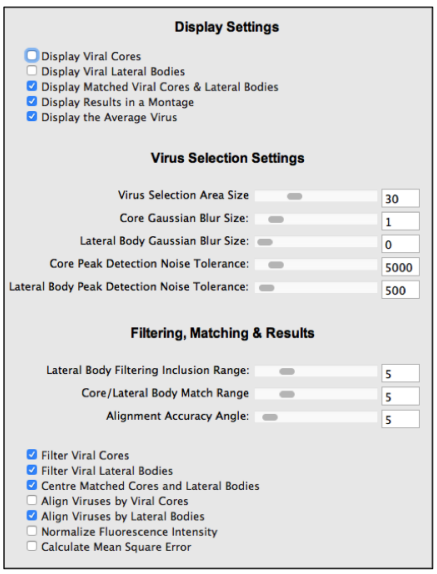

Figure 15: A section of the program's graphical user interface.

3.5 Future Directions

Future directions for this project can be split into two distinct disciplines, computational and biological sciences. Computational future directions for this project begin with improving the general stability of the program, and simplifying the code. The program could then be rewritten in a lower level language, i.e. Java, to significantly improve computation times, and could be rewritten to reduce its dependance on the ImageJ API, which can be error prone and unpredictable in certain cases. A key focus could then be to work on improving the alignment and centering functionality of the program, potentially by analysing the structure of the lateral bodies based on the boundaries of emitted fluorescence. Lastly, the program could be extended to include and analyse 3D SIM image stacks, thereby providing richer data on the localisation of specific proteins of interest.

Biologically, the research can be tackled from the perspective of a data collection project, as to create a structural map of the Vaccinia virion, a significant amount of work will be required in labelling and imaging each identified structural protein. This will theoretically create a detailed map of the Vaccinia virion, where gaps in the map can be investigated to gain further insight into its structural complexity. This process can then be run over a large collection of datasets to enable a representative analysis of structural variation.

4 Conclusions

With this project, we set out to create a simple-to-use tool for wet-laboratory biologists, wherein they could provide it with a selection of raw SIM images, and from there, automatically produce structural models of the virions contained within those images. We feel that these goals were met, with the finished program existing as a lightweight, easily accessible tool, that carries out those aforementioned tasks. The output of this program can be easily manipulated through a simple GUI, producing a variety of useful image selections for further analysis by the biologist.

Although the program has faults within its alignment and centering methodologies, we feel that these faults are overshadowed by the codebase that we provided, which can be further iterated and improved upon in future work.

Future research in this area, along with this program, will allow us to improve the resolution and accuracy of the structural maps that we prototyped in this report, moving us ever closer to a point at which Vaccinia's structural complexity can be unmasked.

References

[1] Richard C. Condit, Nissin Moussatche, and Paula Traktman. In A Nutshell: Structure and Assembly of the Vaccinia Virion, 2006.

[2] Ariella M. Rosengard. Smallpox: the fight to eradicate a global scourge. *Journal of Clinical Investigation*, 112:1775, 2003.

[3] Che-Sheng Chung, Chein-Hung Chen, Ming-Yi Ho, Cheng-Yen Huang, Chung-Lin Liao, and Wen Chang. Vaccinia Virus Proteome: Identification of Proteins in Vaccinia Virus Intracellular Mature Virion Particles. *Journal of Virology*, 80(5):2127–2140, December 2005.

[4] K Pedersen, E J Snijder, S Schleich, N Roos, G Griffiths, and J K Locker. Characterization of vaccinia virus intracellular cores: implications for viral uncoating and core structure. *Journal of virology*, 74(8):3525–3536, April 2000.

[5] S McCraith, T Holtzman, B Moss, and S Fields. Genome-wide analysis of vaccinia virus protein-protein interactions. *Proceedings of the National Academy of Sciences of the United States of America*, 97:4879–4884, 2000.

[6] A J Malkin, A McPherson, and P D Gershon. Structure of intracellular mature vaccinia virus visualized by in situ atomic force microscopy. *Journal of virology*, 77:6332–6340, 2003.

[7] Jaewook Oh and Steven S Broyles. Host cell nuclear proteins are recruited to cytoplasmic vaccinia virus replication complexes. *Journal of virology*, 79:12852–12860, 2005.

[8] N Tolonen, L Doglio, S Schleich, and J Krijnse Locker. Vaccinia virus DNA replication occurs in endoplasmic reticulum-enclosed cytoplasmic mini-nuclei. *Molecular biology of the cell*, 12:2031–2046, 2001.

[9] Y Kuznetsov, P D Gershon, and A McPherson. Atomic force microscopy investigation of vaccinia virus structure. *Journal of virology*, 82:7551–7566, 2008.

[10] R H Green, T F Anderson, and J E Smadel. Morphological Structure of the Virus of Vaccinia. *The Journal of experimental medicine*, 75:651–656, 1942.

[11] G V Stokes. High-voltage electron microscope study of the release of vaccinia virus from whole cells. *Journal of virology*, 18:636–643, 1976.

[12] John Heuser. Deep-etch EM reveals that the early poxvirus envelope is a single membrane bilayer stabilized by a geodetic "honeycomb" surface coat. *Journal of Cell Biology*, 169:269–283, 2005.

[13] Marek Cyrklaff, Cristina Risco, Jose Jesús Fernández, Maria Victoria Jiménez, Mariano Estéban, Wolfgang Baumeister, and José L Carrascosa. Cryo-electron tomography of vaccinia virus. *Proceedings of the National Academy of Sciences of the United States of America*, 102:2772–2777, 2005.

[14] G Griffiths, R Wepf, T Wendt, J K Locker, M Cyrklaff, and N Roos. Structure and assembly of intracellular mature vaccinia virus: isolated-particle analysis. *Journal of virology*, 75:11034–11055, 2001.

[15] Desyree Murta Jesus, Nissin Moussatche, and Richard C Condit. Vaccinia virus mutations in the L4R gene encoding a virion structural protein produce abnormal mature particles lacking a nucleocapsid. *Journal of virology*, 88(24):14017–14029, December 2014.

[16] FlorianIngo Schmidt, ChristopherKarlErnst Bleck, Lucia Reh, Karel Novy, Bernd Wollscheid, Ari Helenius, Henning Stahlberg, and Jason Mercer. Vaccinia virus entry is followed by core activation and proteasome-mediated release of the immunomodulatory effector VH1 from lateral bodies. *Cell Reports*, 4:464–476, 2013.

[17] J.A. Holowczak, Virginia L. Thomas, and Lizabeth Flores. Isolation and characterization of vaccinia virus nucleoids. *Virology*, 67(2):506–519, October 1975.

[18] Che-Sheng Chung, Chein-Hung Chen, Ming-Yi Ho, Cheng-Yen Huang, Chung-Lin Liao, and Wen Chang. Vaccinia virus proteome: identification of proteins in vaccinia virus intracellular mature virion particles. *Journal of virology*, 80:2127–2140, 2006.

[19] O N Jensen, T Houthaeve, A Shevchenko, S Cudmore, T Ashford, M Mann, G Griffiths, and J Krijnse Locker. Identification of the major membrane and core proteins of vaccinia virus by two-dimensional electrophoresis. *Journal of virology*, 70:7485–7497, 1996.

[20] Adrien Breiman and Geoffrey L. Smith. Vaccinia virus B5 protein affects the glycosylation, localization and stability of the A34 protein. *Journal of General Virology*, 91:1823–1827, 2010.

[21] Jacquelyn Horsington, Lynne Turnbull, Cynthia B. Whitchurch, and Timothy P. Newsome. Subviral imaging of vaccinia virus using super-resolution microscopy. *Journal of Virological Methods*, 186:132–136, 2012.

[22] Johannes Schindelin, Ignacio Arganda-Carreras, Erwin Frise, Verena Kaynig, Mark Longair, Tobias Pietzsch, Stephan Preibisch, Curtis Rueden, Stephan Saalfeld, Benjamin Schmid, Jean-Yves Tinevez, Daniel James White, Volker Hartenstein, Kevin Eliceiri, Pavel Tomancak, and Albert Cardona. Fiji: an open-source platform for biological-image analysis, 2012.